New Insights into Low-Temperature Oxidation of Propane from Synchrotron Photoionization Mass Spectrometry and Multi-Scale Informatics Modeling

ARTICLE *in* THE JOURNAL OF PHYSICAL CHEMISTRY A · APRIL 2015

Impact Factor: 2.69 · DOI: 10.1021/acs.jpca.5b01008 · Source: PubMed

9 AUTHORS, INCLUDING:

Oliver Welz
BASF SE
46 PUBLICATIONS **640** CITATIONS
SEE PROFILE

John D Savee
Los Gatos Research
49 PUBLICATIONS **632** CITATIONS
SEE PROFILE

David Osborn
Sandia National Laboratories
121 PUBLICATIONS **2,293** CITATIONS
SEE PROFILE

Craig A Taatjes
Sandia National Laboratories
200 PUBLICATIONS **4,392** CITATIONS
SEE PROFILE

THE JOURNAL OF PHYSICAL CHEMISTRY A

Article

pubs.acs.org/JPCA

New Insights into Low-Temperature Oxidation of Propane from Synchrotron Photoionization Mass Spectrometry and Multiscale Informatics Modeling

Oliver Welz,*[,†,∥] Michael P. Burke,[‡,§] Ivan O. Antonov,[†] C. Franklin Goldsmith,[‡,⊥] John D. Savee,[†] David L. Osborn,[†] Craig A. Taatjes,[†] Stephen J. Klippenstein,[‡] and Leonid Sheps*[,†]

[†]Combustion Research Facility, Sandia National Laboratories, Livermore, California 94551, United States

[‡]Chemical Sciences and Engineering Division, Argonne National Laboratory, Argonne, Illinois 60493, United States

[§]Department of Mechanical Engineering, Department of Chemical Engineering and Data Sciences Institute, Columbia University, New York, New York 10027, United States

Supporting Information

ABSTRACT: Low-temperature propane oxidation was studied at P = 4 Torr and T = 530, 600, and 670 K by time-resolved multiplexed photoionization mass spectrometry (MPIMS), which probes the reactants, intermediates, and products with isomeric selectivity using tunable synchrotron vacuum UV ionizing radiation. The oxidation is initiated by pulsed laser photolysis of oxalyl chloride, $(COCl)_2$, at 248 nm, which rapidly generates a ~1:1 mixture of 1-propyl (*n*-propyl) and 2-propyl (*i*-propyl) radicals via the fast Cl + propane reaction. At all three temperatures, the major stable product species is propene, formed in the propyl + O_2 reactions by direct HO_2 elimination from both *n*- and *i*-propyl peroxy radicals. The experimentally derived propene yields relative to the initial concentration of Cl atoms are (20 ± 4)% at 530 K, (55 ± 11)% at 600 K, and (86 ± 17)% at 670 K at a reaction time of 20 ms. The lower yield of propene at low temperature reflects substantial formation of propyl peroxy radicals, which do not completely decompose on the experimental time scale. In addition, C_3H_6O isomers methyloxirane, oxetane, acetone, and propanal are detected as minor products. Our measured yields of oxetane and methyloxirane, which are coproducts of OH radicals, suggest a revision of the OH formation pathways in models of low-temperature propane oxidation. The experimental results are modeled and interpreted using a multiscale informatics approach, presented in detail in a separate publication (Burke, M. P.; Goldsmith, C. F.; Klippenstein, S. J.; Welz, O.; Huang H.; Antonov I. O.; Savee J. D.; Osborn D. L.; Zádor, J.; Taatjes, C. A.; Sheps, L. Multiscale Informatics for Low-Temperature Propane Oxidation: Further Complexities in Studies of Complex Reactions. *J. Phys. Chem. A.* **2015**, DOI: 10.1021/acs.jpca.5b01003). The model predicts the time profiles and yields of the experimentally observed primary products well, and shows satisfactory agreement for products formed mostly via secondary radical−radical reactions.

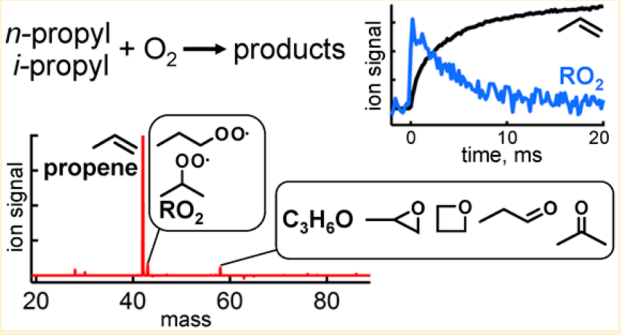

INTRODUCTION

Low-temperature (T < ~900 K) oxidation chemistry plays an important role in the autoignition processes that, e.g., govern performance of internal combustion engines.[1] The chain branching and heat release at low temperature influences when the reacting system is driven into hot ignition.[2] Autoignition is unwanted in spark-ignition engines because it is associated with engine knock. In contrast, advanced engine designs (such as homogeneous charge compression ignition) rely on autoignition and are exquisitely sensitive to fuel-chemistry effects in low-temperature oxidation reactions.[3] For comprehensive combustion models to reliably predict autoignition, the underlying complex chemical kinetics must be understood in detail.

A key part of low-temperature oxidation of alkanes (RH) starts with the reaction of initial fuel radicals R with O_2 to form chemically activated alkyl peroxy (RO_2) species:

$$R + O_2 \rightleftarrows RO_2 \quad (R1)$$

$$RO_2 \rightarrow HO_2 + R_{-H} \quad (R2)$$

$$RO_2 \rightleftarrows QOOH \quad (R3)$$

Special Issue: 100 Years of Combustion Kinetics at Argonne: A Festschrift for Lawrence B. Harding, Joe V. Michael, and Albert F. Wagner

Received: January 30, 2015
Revised: April 5, 2015
Published: April 10, 2015

DOI: 10.1021/acs.jpca.5b01008
J. Phys. Chem. A 2015, 119, 7116−7129

$$\text{QOOH} \rightarrow \text{OH} + \text{oxygenated species} \quad \text{(R4)}$$

$$\text{QOOH} + \text{O}_2 \rightleftarrows \text{OOQOOH} \quad \text{(R5)}$$

$$\text{OOQOOH} \rightarrow \text{OH} + \text{ketohydroperoxide} \quad \text{(R6)}$$

$$\text{ketohydroperoxide} \rightarrow \text{OH} + \text{alkoxy radical} \quad \text{(R7)}$$

At low temperature and sufficiently high pressure RO_2 radicals are efficiently stabilized by molecular collisions. As temperature increases, unimolecular RO_2 decomposition channels become available, with the major product pathway typically being direct elimination of HO_2 via a five-membered cyclic transition state, producing stable alkene coproducts.[4,5] Such pathways are essentially radical chain-terminating in the low-temperature regime, where HO_2 is relatively unreactive. Alternatively, RO_2 can isomerize to carbon-centered hydroperoxyalkyl radicals (QOOH), which subsequently decompose or react with O_2 to yield hydroperoxyalkyl peroxy radicals (OOQOOH). QOOH decomposition forms primarily OH + cyclic ethers (a chain-propagating step[1]), whereas second O_2 addition to QOOH can eventually lead to chain-branching production of 2 OH + alkoxy radical coproduct (reactions R5−R7).[1,6] A more comprehensive discussion of product channels from OOQOOH and from ketohydroperoxide specifically for propane as the fuel has been recently published.[7,8]

The kinetics of alkyl + O_2 reactions involves a competition of sequential pathways, which proceed by transitions between adjacent potential wells, and "formally direct" pathways, which pass multiple transition states without stabilization in the intermediate wells. For example, one possible formally direct pathway is

$$\text{R} + \text{O}_2 \rightarrow \text{OH} + \text{oxygenated species} \quad \text{(R8)}$$

which involves a chemically activated sequence R + O_2 → RO_2 → QOOH → OH + oxygenated species without stabilization of either RO_2 or QOOH intermediates. Establishing accurate kinetics models that capture the temperature and pressure dependence of this complex network of reaction pathways is crucial to building rigorous combustion mechanisms.

The propyl + O_2 reaction is a prototype for larger alkane oxidation because it exhibits many of the mechanistic features typical for the reactions of larger alkyl radicals with O_2. At the same time, this system is small enough to allow both a high-level theoretical treatment and a rigorous interpretation of the experimental results. Consequently, it has been extensively studied both experimentally[9−23] and computationally.[7,19−31] Previous experimental studies of the propyl + O_2 reaction included quantification of stable species in steady-state reactors[9,15−17,23] as well as time-resolved measurements of propyl radicals, propene, OH, and HO_2.[12−14,18−22,24,32]

The earliest steady-state experiments by Baker et al.[9] showed that propene is the major stable product in propyl oxidation, using gas-chromatographic (GC) analysis of propane added to a slowly reacting mixture of H_2/O_2 at P = 500 Torr, T = 753 K. Four C_3H_6O isomers were identified: oxetane, propanal, and methyloxirane were assigned as primary oxidation products, but acetone was thought to arise mostly from secondary chemistry. More recently, Cord et al.[23] quantified products of low-temperature propane oxidation in a jet-stirred reactor at P = 795 Torr and T = 530−730 K using both GC and synchrotron photoionization mass spectrometry. Their model successfully reproduced the main oxidation products, but showed larger discrepancies with measurements of minor and secondary products.

Slagle et al. investigated the kinetics of the n-C_3H_7 + O_2[13] and i-C_3H_7 + O_2[14] reactions at low pressures (∼0.5−7 Torr) using laser photolysis in a flow reactor and time-resolved photoionization mass spectrometry with fixed-wavelength discharge lamps for detection of propyl radicals and C_3H_6. For the n-C_3H_7 + O_2 reaction, Slagle et al. reported rising propene yields from ∼0.14 at 550 K to >0.8 at 635 K, evidence of the increased role of thermal decomposition of propyl peroxy radicals. In addition, time-resolved detection provided the first hints of the competition between rapid formally direct and slower thermal propene formation.[13]

Taatjes and co-workers used laser-spectroscopic methods to probe the time-resolved formation of OH[19,22,32] or HO_2[18,20,21,24] in propyl oxidation at pressures up to 60 Torr and temperatures up to 700 K, revealing the competition between prompt and thermal product channels. The experimental OH and HO_2 time traces were modeled with rate coefficients derived from *ab initio*-based time-dependent multiple-well master-equation calculations on the n-C_3H_7 + O_2 and i-C_3H_7 + O_2 potential energy surfaces (PESs). Adjustments of the energies of key minima and first-order saddle points within the uncertainties of the quantum-chemical methods allowed for satisfactory agreement between the experimental and modeled time traces.

In the present study, we investigate propane oxidation between 530 and 670 K at 4 Torr using pulsed-photolytic Cl atom initiation[24] and time-resolved multiplexed synchrotron photoionization mass spectrometry (MPIMS). This approach provides the advantage of simultaneous direct time-resolved detection of multiple stable products as well as transient intermediates with isomeric selectivity. Crucially, we extend the earlier time-resolved studies of OH and HO_2 formation by detecting the stable coproducts associated with these channels. Formation of OH in the propyl + O_2 reaction can occur via several pathways associated with different oxygenated coproducts (methyloxirane, oxetane, acetone and propanal), and their detection allows us to probe the individual OH-forming channels directly.

The experimental results are modeled and interpreted based on the multiscale informatics (MSI) approach introduced by Burke et al.,[33] applied to the propyl + O_2 system. The present paper focuses on the analysis and mechanistic interpretation of the experimental results aided by the MSI model. Details about the modeling methodology are presented in a second paper.[34]

EXPERIMENTAL METHODS

MPIMS experiments employed synchrotron-generated vacuum-ultraviolet (VUV) ionization radiation from the Chemical Dynamics Beamline at the Advanced Light Source of Lawrence Berkeley National Laboratory. Details of the setup can be found in previous publications,[35−37] and only a brief summary is given here. The reaction occurred in a slow-flow heatable (300−1000 K) low-pressure (1−10 Torr) quartz tube with an inner diameter of 1.05 cm and a length of 62 cm. Metered flows of propane (C_3H_8), O_2, and the Cl atom precursor oxalyl chloride $(COCl)_2$, all diluted in helium bath gas, were introduced by calibrated mass flow controllers and mixed in situ at the entrance of the reactor. An excimer laser operating at 248 nm with a repetition rate of either 4 or 10 Hz fired along the reactor axis and created a uniform Cl atom profile in both axial

DOI: 10.1021/acs.jpca.5b01008
J. Phys. Chem. A 2015, 119, 7116−7129

Table 1. Experimental Conditions during the Photoionization Energy Scans

T (K)	P (Torr)	[He] (cm^{-3})	[O_2] (cm^{-3})	[C_3H_8] (cm^{-3})	[$(COCl)_2$] (cm^{-3})	$[Cl]_0$ (cm^{-3})
530	4.0	6.2×10^{16}	9.8×10^{15}	9.8×10^{14}	1.3×10^{14}	6.7×10^{12}
600	4.0	5.3×10^{16}	1.0×10^{16}	1.0×10^{15}	1.3×10^{14}	7.0×10^{12}
670	4.0	4.6×10^{16}	1.0×10^{16}	1.0×10^{15}	1.3×10^{14}	8.2×10^{12}

and radial dimensions of the reactor. Typical laser fluences were ~85 mJ cm^{-2}.

The pressure inside the reactor was maintained at 4 Torr using a butterfly valve in the exhaust line with active feedback control, and experiments were done at temperatures of 530, 600, and 670 K. The initial Cl atom concentration $[Cl]_0$ from photolysis of $(COCl)_2$ was calculated based on the concentration of $(COCl)_2$ in the reactor and its measured depletion after photolysis, using a quantum yield $\Phi = 2$ for Cl atom formation at 248 nm.[38] The experimental conditions for the main data set, consisting of photoionization energy scans, are given in Table 1. Additional survey experiments, designed to identify which mass peaks arise from radical−radical reactions, were done at selected fixed photon energies, either increasing [O_2] (by up to a factor of 5.4) or reducing $[Cl]_0$ (by a factor of 3) while maintaining a total pressure of 4 Torr.

The reacting mixture was continuously sampled through a 650 μm-diameter pinhole in the reactor sidewall into a vacuum chamber, skimmed, and crossed with tunable VUV synchrotron ionizing radiation. The resulting cations were collimated and detected as a function of their mass-to-charge (m/z) ratio in an orthogonal extraction time-of-flight mass spectrometer. The mass resolution of the spectrometer, $m/\Delta m \approx 1500$, was sufficient to distinguish products with the same nominal mass, but different elemental composition, such as C_2H_4O (m/z = 44.03) and C_3H_8 (m/z = 44.06). At a given photoionization energy E, full mass spectra were acquired in intervals of 20 μs from reaction times $t = -20$ to 130 ms (4 Hz repetition rate) or $t = -10$ to 40 ms (10 Hz repetition rate) relative to photolysis, resulting in time-resolved mass spectra $I(m/z, t)$. Additionally, the energy of the ionizing photons was scanned in steps of 25 meV over the range 9.2−11.2 eV, leading to a three-dimensional data set $I(m/z, t, E)$. All ion signals were normalized to the photon flux of the ionizing radiation using a NIST-calibrated photodiode.

By scanning the energy of the ionizing radiation, species can be identified and quantified at an isomer-resolved level. The analysis of the experimental data is in large part analogous to the analysis presented in ref 39. Briefly, the ion intensity at any m/z value is a sum of signals from all isomers of molecular mass m:

$$S_{m/z}^{(t,t+\Delta t)}(E) = \alpha_{m/z} \cdot \Lambda \cdot \sum_i [\sigma_i(E) \cdot c_i^{(t,t+\Delta t)}] \quad (1)$$

In eq 1, $S_{m/z}^{(t,t+\Delta t)}(E)$ is the ion signal, integrated over kinetic times $(t, t + \Delta t)$ and normalized to the photon flux at ionization energy E, $c_i^{(t,t+\Delta t)}$ is the concentration of isomer i in the reactor, and $\sigma_i(E)$ is its partial photoionization cross section at a given m/z. The quantity $\alpha_{m/z}$ is an isomer-independent mass discrimination factor, and Λ is a mass- and photon energy-independent instrument sensitivity factor.[37] We measured $\alpha_{m/z}$ directly using calibration gas mixtures and determined the parametrization $\alpha_{m/z} = m_i^{0.60}$ for parent ions under our experimental conditions. Referencing all ion signals to propane, whose absolute concentration is known, allows the determination of Λ and the quantification of any other species with a known ionization cross-section. In the current work, we determined the absolute photoionization cross sections of propane, acetone, oxetane, and methyloxirane employing the procedure described in detail in ref 40. Published cross-section data were taken from previous measurements for methyl,[37] ethene,[39] formaldehyde,[41] hydrogen peroxide,[42] propene,[40] acetaldehyde,[40] and propanal.[43]

Time-resolved absolute species concentrations were derived using the procedure outlined in ref 39. For all products quantified except the C_3H_6O isomers, parent ion signals consisted only of a single isomer, so that their concentration profiles were readily calculated from time-resolved ion traces. The C_3H_6O product signal is more complex, because four isomers—oxetane (ionization energy (IE): 9.65 eV),[44] acetone (IE: 9.70 eV),[44] propanal (IE: 9.96 eV),[44] and methyloxirane (IE: 10.22 eV)[44]—contribute to the overall C_3H_6O time profile. To extract isomer-resolved time traces, we performed experiments at selected photon energies: 9.85 eV, where only acetone and oxetane contribute; 10.05 eV, which includes additional contribution from propanal; and 11 eV, where all four isomers contribute. The similar IEs of acetone and oxetane made time-resolved measurements of oxetane alone impractical, since they required long averaging of very weak signals at the ionization threshold of oxetane (below the IE of acetone, 9.70 eV). Therefore, in further analysis we treat the time profiles of acetone and oxetane as identical. Photoionization spectra integrated over a range of reaction times (see below) have sufficient signal-to-noise ratio to show that the total time-integrated yield (up to t = 30 ms) of oxetane is negligible at 530 K, and is <5% of the C_3H_6O isomers at 600 K. Likewise, acetone accounts for <4% of the total C_3H_6O production (up to t = 20 ms) at 670 K. Consequently, our assumption of identical time evolution for acetone and oxetane has at most a minor effect on the overall results. This assumption is also supported by the similar relative yield of oxetane and acetone (within the error bars), when integrated over early (0−15 ms) or late (10−25 ms) reaction times at 670 K. To obtain the time profile of propanal, we subtracted the contribution of acetone and oxetane from the 10.05 eV data. Correspondingly, the methyloxirane time profile was obtained by subtracting contributions from acetone, oxetane, and propanal from the 11 eV data.

THEORY AND MODELING METHODS

Model predictions and interpretations given below employ a model constructed using the MSI approach.[33,34] The MSI framework incorporates a wide range of chemical complexity, from fundamental molecular interactions (such as reaction barrier heights) to global observable phenomena (such as product yields). It allows self-consistent integration of diverse data types: ab initio calculations, experimental determinations of reaction rate coefficients, and species concentration measurements. Complete details of the approach and implementation are provided in our companion paper,[34] though we highlight some of the key features here.

DOI: 10.1021/acs.jpca.5b01008
J. Phys. Chem. A 2015, 119, 7116−7129

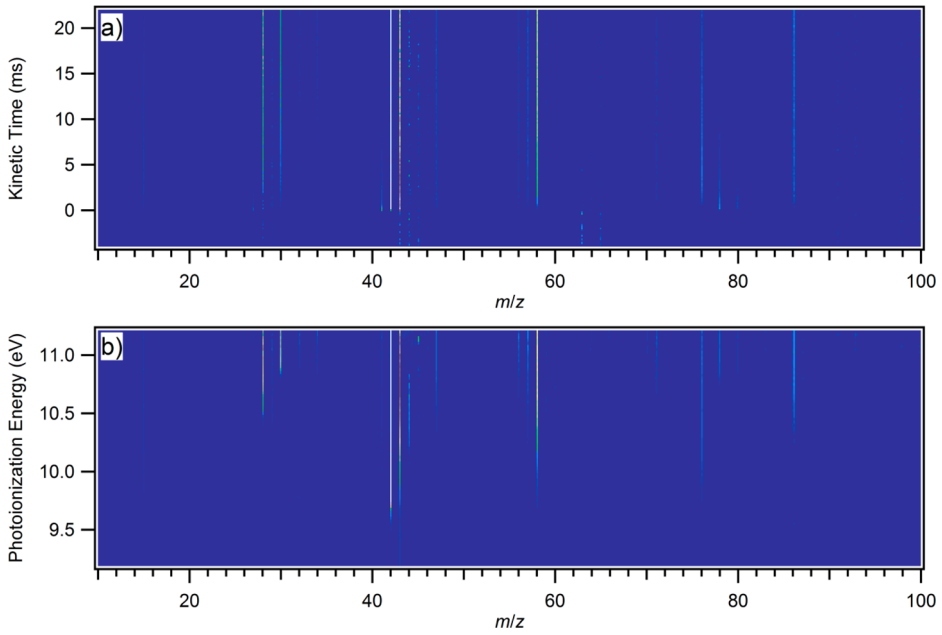

Figure 1. (a) Time-resolved product mass spectrum integrated over photon energies 9.2−11.2 eV and (b) mass-resolved product photoionization spectrum integrated over kinetic times 0−20 ms after photolysis for propane oxidation at 670 K and 4 Torr. The photolysis laser fires at $t = 0$. Only the signal related to product formation is shown; the signal arising from photolysis of oxalyl chloride and reactive removal of propane is omitted for clarity.

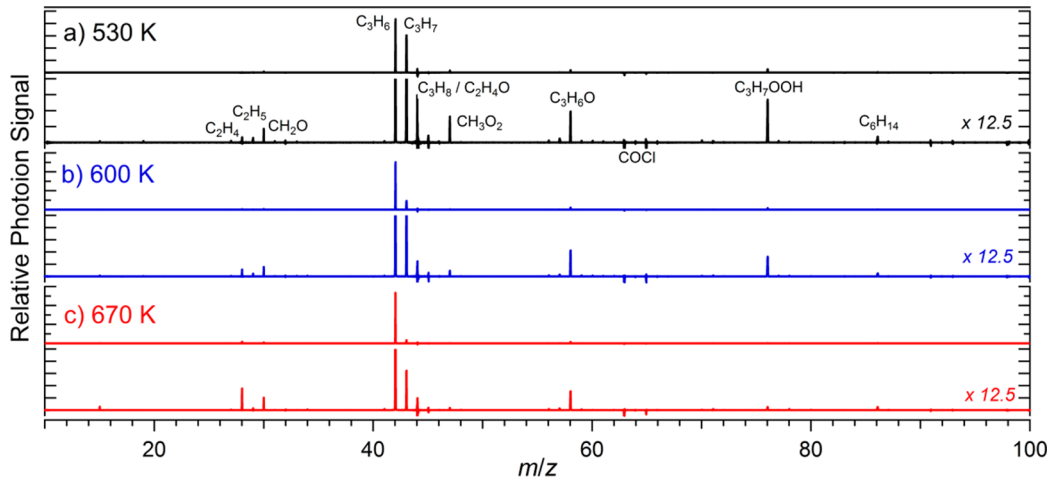

Figure 2. Transient mass spectra (after subtraction of pre-photolysis signal) for propane oxidation at 4 Torr at (a) 530 K, (b) 600 K, and (c) 670 K, integrated over photon energies 9.2−11.2 eV and kinetic times 0−30 ms (530 and 600 K) and 0−20 ms (670 K). For each temperature, the mass spectra are also shown enlarged by a factor of 12.5 to emphasize minor product peaks.

A core starting (*a priori*) model was first constructed by layering various submodels describing reactions among C_0−C_3 species, notably including theoretical results of Goldsmith et al.[7] for R + O_2 and QOOH + O_2 reaction systems related to propyl radical oxidation. In the MSI model, the R + O_2 and QOOH + O_2 systems, along with a selected set of ∼30 secondary reactions, are treated actively in an iterative fit. Active variables are assigned to describe uncertain theoretical kinetics parameters (barrier heights, average energies transferred per collision, partition functions, etc.), rate coefficient parameters, and experimental conditions (initial/boundary conditions, absorption cross sections, physical model assumptions, etc.). The active parameters are subsequently optimized against a selected set of targets, for which model prediction uncertainties are primarily attributable to the R + O_2 and QOOH + O_2 reaction systems. These targets include ab initio calculated molecular properties from Goldsmith et al.[7] for R + O_2 and QOOH + O_2 reactions; reported secondary reaction rate coefficients (where available); earlier time-resolved measurements of OH,[22] HO_2,[18] *n*-propyl,[13] and *i*-propyl;[12] new time-resolved measurements of OH;[34] measurements of C_3H_6, oxetane, and methyloxirane from the present study; and reported values for the experimental conditions employed in those studies. Other species measured here (e.g., CH_3, C_2H_4), for which model prediction uncertainties show non-negligible contributions from secondary reactions, are not included as optimization targets. However, these measurements will be useful in future modeling efforts focused on improved quantification of the relevant secondary reactions.

DOI: 10.1021/acs.jpca.5b01008
J. Phys. Chem. A 2015, 119, 7116−7129

Table 2. Experimentally Identified Products at T = 530, 600, and 670 K, and P = 4 Torr[a]

			concentration at t = 20 ms/10^{10} cm^{-3}		
m/z	formula	species	530 K	600 K	670 K
15	CH_3	methyl	0.37 ± 0.09	0.75 ± 0.19	2.9 ± 0.6
28	C_2H_4	ethene	3.0 ± 0.8	11.9 ± 2.7	97 ± 20
29	C_2H_5	ethyl			
	$C_2H_5O_2$[b]	ethyl peroxy			
30	CH_2O	formaldehyde	16 ± 4	35 ± 8	86 ± 19
34	H_2O_2	hydrogen peroxide			
42	C_3H_6	propene	134 ± 27	390 ± 80	710 ± 150
43	C_3H_7	*n*-propyl, *i*-propyl			
	$C_3H_7O_2$[b]	*n*-propyl, *i*-propyl peroxy			
44	C_2H_4O	acetaldehyde	8.1 ± 2.0	8.9 ± 2.1	9.1 ± 2.1
47	CH_3O_2	methyl peroxy			
58	C_3H_6O	acetone	1.4 ± 0.8	2.5 ± 0.9	1.1 ± 0.8
		propanal	3.9 ± 0.9	8.3 ± 2.3	6.0 ± 1.6
		oxetane	<0.17[c]	1.0 ± 0.8	3.7 ± 1.5
		methyloxirane	3.2 ± 0.9	9.8 ± 2.6	18.4 ± 4.2
60	C_3H_7OH	*n*-propanol, *i*-propanol			
76	$C_3H_8O_2$	*n*-propyl, *i*-propyl hydroperoxide			
86	C_6H_{14}	C_6H_{14} isomers			

[a]Absolute concentrations of species, for which photoionization cross sections are available are given at kinetic time t = 20 ms. The cited errors are sums of the estimated uncertainties in the absolute photoionization cross sections (20%) and the 1σ uncertainties from fitting the experimental product spectra according to eq 1. [b]$C_2H_5O_2$ and $C_3H_7O_2$ do not produce ion signal at their parent ion mass; they are detected via their fragment ions $C_2H_5^+$ and $C_3H_7^+$, respectively. [c]The fit to the C_3H_6O photoionization product spectrum at 530 K predicts a negligible yield of oxetane. The upper bound given here represents the uncertainty from this fit.

Improved values for uncertain model parameters and the covariance matrix are calculated from an iterative, least-squares error minimization. The final multiscale informed kinetics model consists of optimized theoretical kinetics parameters (with constrained uncertainties), related through kinetics calculations to temperature/pressure/bath gas-dependent rate constants, which in turn are related through physical models to global observable behavior (with uncertainties propagated throughout). Estimated uncertainties shown below reflect propagated uncertainties from active parameters only; estimated uncertainties for species (e.g., CH_3, C_2H_4), for which model predictions show high sensitivity to secondary reactions not considered in the active set, are likely underestimates of the model uncertainty since those uncertainties are not properly quantified. For the purposes of comparison, model predictions are also conducted using the R + O_2 reaction treatment of Huang et al.[22] substituted into the *a priori* model.

RESULTS AND DISCUSSION

Figure 1a,b shows a time-resolved mass spectrum and a mass-resolved photoionization spectrum of Cl-initiated propane oxidation at 4 Torr and 670 K. 248 nm photolysis of oxalyl chloride instantaneously generates Cl atoms, which rapidly react with propane to form a nearly equal parts mixture of *n*-C_3H_7 and *i*-C_3H_7 radicals. The *n*-/*i*-propyl ratio changes from 50:50 at 530 K to 52:48 at 670 K in the optimized MSI model, in near-perfect agreement with extrapolations based on available literature data at T up to 467 K.[45−48] Under our experimental conditions, the propyl radicals react mostly with O_2 and eventually form products via RO_2 chemistry. Figure 2 shows mass spectra at 530, 600, and 670 K, obtained by integration over a range of kinetic times and photon energies. The pre-photolysis ion signals have been subtracted, so that positive peaks reflect the formation of products, and negative peaks indicate reactive removal of propane (C_3H_8) at m/z = 44 and photolytic depletion of oxalyl chloride. Note that the mass spectra are plotted only up to m/z = 100 for clarity, so that parent ion signals of oxalyl chloride (m/z = 126 ($C_2O_2{}^{35}Cl_2$), 128 ($C_2O_2{}^{35}Cl^{37}Cl$), 130 ($C_2O_2{}^{37}Cl_2$)) are not shown. Nevertheless, photodissociation of oxalyl chloride is evident in Figure 2 by the depletion of its fragment ion peaks at m/z = 63 and 65 ($CO^{35}Cl$ and $CO^{37}Cl$). In all, we identified numerous product and intermediate species contributing to the transient signals, summarized in Table 2. Of these, we quantified nine compounds based on their photoionization cross sections, and the absolute concentrations of these species at reaction time t = 20 ms are also included in Table 2.

Identification of Products. The PESs for the *n*-C_3H_7 + O_2 and *i*-C_3H_7 + O_2 reactions[7] are shown in Figures 3 and 4, respectively. Based on these surfaces, propene (m/z = 42) and the C_3H_6O (m/z = 58) isomers methyloxirane, oxetane, propanal, and acetone are the expected primary closed-shell

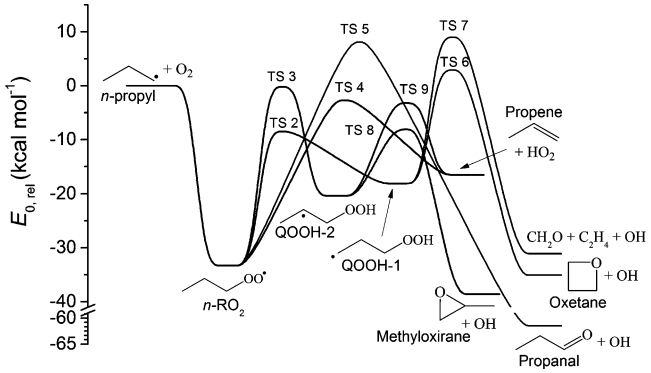

Figure 3. Calculated stationary points on the potential energy surface for the *n*-C_3H_7 + O_2 reaction. The energies, relative to the reactants at 0 K, are from Goldsmith et al.[7]

DOI: 10.1021/acs.jpca.5b01008
J. Phys. Chem. A 2015, 119, 7116−7129

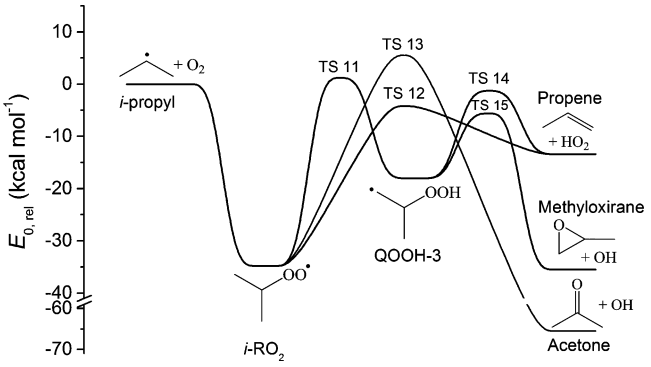

Figure 4. Calculated stationary points on the potential energy surface for the *i*-C_3H_7 + O_2 reaction. The energies, relative to the reactants at 0 K, are from Goldsmith et al.[7]

products. Their formation competes with secondary reactions and with stabilization of *n*- and *i*-propyl peroxy (*n*-$C_3H_7O_2$ and *i*-$C_3H_7O_2$) radicals, which are detected through dissociative ionization[49] at m/z = 43. Experiments performed with initial radical concentrations reduced by a factor of 3 show that only the ion signals at masses 42, 43, and 58 scale approximately linearly with $[Cl]_0$, consistent with our expectations of their formation via primary R + O_2 chemistry.

According to Figure 2, the most intense product signal occurs at m/z = 42 (C_3H_6) and 43 (C_3H_7) at all three temperatures. A comparison of the C_3H_6 photoionization product spectra with a calibration spectrum of propene[40] (Figure S1) identifies it as the only contribution at all experimental conditions. As shown in Table 2, propene is by far the most prominent stable product observed at all three temperatures. The m/z = 43 product ion signal is a combination of direct ionization of *n*- and *i*-propyl radicals and dissociative ionization of the propyl peroxy radical isomers, which lose a neutral O_2 fragment upon photoionization.[50] Based on the photoionization spectra, the appearance energy of $C_3H_7^+$ from ionization of $C_3H_7O_2$ is ~9.7 eV, well above the IEs of *n*-C_3H_7 (8.1 eV) and *i*-C_3H_7 (7.4 eV).[51] As a result, signal below 9.7 eV is caused by propyl radicals alone, whereas signal above 9.7 eV arises from both compounds, with a dominant contribution from the propyl peroxy radicals. Figure S2 shows the time profile of the C_3H_7 ion signal as a function of photon energy at 530 K and 4 Torr. Under our experimental conditions, propyl radicals are formed by the reaction of Cl with propane[47] within <10 μs after the photolysis pulse and then rapidly consumed by reaction with O_2.[7] In contrast, the time profile of propyl peroxy radicals shows a plateau toward later times, suggesting that propyl peroxy radicals are thermally stable on the experimental time scale at 530 K.

Relative to the intense signal of propene and propyl peroxy, signal at m/z = 58 associated with the C_3H_6O isomers is small, suggesting that formation of C_3H_6O + OH is a minor channel in propyl oxidation under our conditions. Comparison of the m/z = 58 photoionization product spectra with calibration spectra of the pure compounds reveals contributions from oxetane, methyloxirane, propanal, and acetone. The product spectrum at 670 K is shown in Figure 5, along with an isomer-resolved simulation according to eq 1. Because the IEs and shapes of the photoionization spectra of propanal (IE = 9.96 eV) and methyloxirane (IE = 10.22 eV) are sufficiently different, these species can be readily identified and quantified. In contrast, the quantification of oxetane and acetone is more

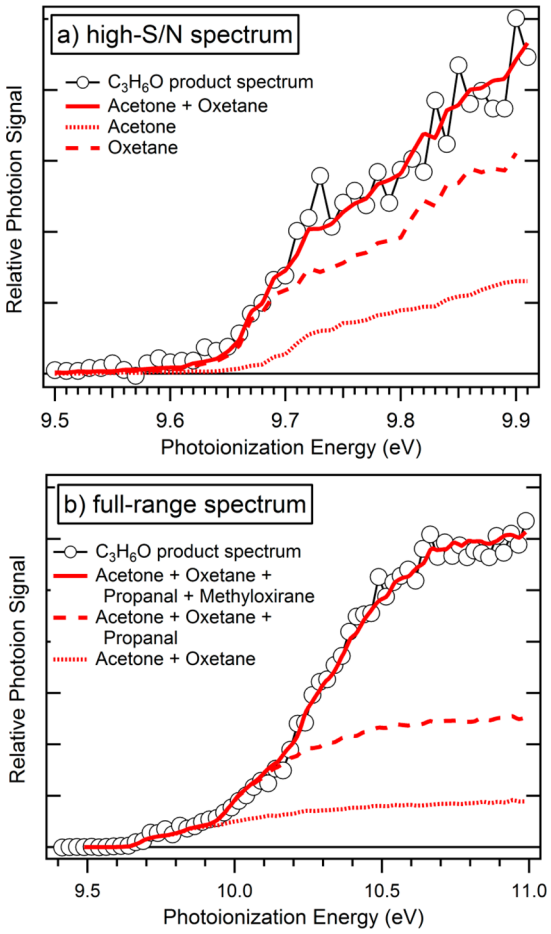

Figure 5. Photoionization spectra of the C_3H_6O product channel at 670 K, along with isomer-resolved simulations. (a) High-S/N spectrum from 9.5 to 9.9 eV, integrated over kinetic times 0–25 ms, to determine the ratio of acetone to oxetane. (b) Full-range spectrum from 9.2 to 11.2 eV, integrated over t = 0 – 20 ms, with additional contributions from propanal and methyloxirane. The ratio of acetone to oxetane was fixed as determined from the high-S/N spectrum.

challenging, because both their IEs (acetone: 9.70 eV, oxetane: 9.65 eV) and shapes of the photoionization spectra are similar. To more reliably determine the relative contributions of acetone and oxetane, we recorded the photoionization spectra at 600 and 670 K from 9.5–9.9 eV with higher signal-to-noise (S/N) ratio (Figure 5a). The ratio of the isomeric contributions derived from these high S/N spectra was kept fixed when fitting the full photoionization spectrum from 9.2–11.2 eV, shown in Figure 5b. At 530 K, the lower-resolution spectrum from 9.2–11.2 eV showed a negligible oxetane yield with enough certainty that a high-S/N photoionization scan at this temperature was not necessary.

Several other minor product peaks are identified, as summarized in Table 2. Except m/z = 29, which contains contributions from dissociative ionization of ethyl peroxy radicals, these peaks correspond to parent ion formation: m/z = 15: methyl (CH_3, quantified); m/z = 28: ethene (C_2H_4, quantified); m/z = 29: ethyl (C_2H_5) and dissociative ionization of ethylperoxy radicals ($C_2H_5O_2$); m/z = 30: formaldehyde (CH_2O, quantified); m/z = 34: hydrogen peroxide (H_2O_2); m/z = 44: acetaldehyde (C_2H_4O, quantified); m/z = 47: methyl peroxy (CH_3O_2); m/z = 60: propanol isomers (C_3H_7OH); m/z = 76: propyl hydroperoxide isomers (C_3H_7OOH); m/z = 86:

DOI: 10.1021/acs.jpca.5b01008
J. Phys. Chem. A 2015, 119, 7116–7129

C_6H_{14} isomers. As discussed below, these products come mostly from secondary radical−radical chemistry, except ethene and CH_3, which are formed at least in part by thermal decomposition of n-C_3H_7 at higher temperature.

Kinetics and Mechanism of the Propyl + O_2 Reaction. In the following sections, we discuss the kinetics and mechanism of primary product formation as well as secondary chemistry in the propyl + O_2 reaction, aided by the MSI modeling results. We note that the MSI approach treats experimental conditions as variables rather than constants; in fact, the optimized MSI model suggests that our initial radical concentrations are ∼10−20% lower than those listed in Table 1. This suggested change is within the experimental uncertainty in $[Cl]_0$ and does not alter any of our conclusions. In the following, we report the measured absolute yields relative to the experimental value of $[Cl]_0$, whereas the mechanistic interpretation of the model outputs is based on the optimized model value of $[Cl]_0$.

Propene and Propyl Peroxy ($C_3H_7O_2$) Radicals. Figure 6 shows the time profiles of propene and m/z = 43 ions (dominated by propyl peroxy radicals, n- and i-$C_3H_7O_2$) at 530, 600, and 670 K, along with a comparison to results from the MSI model. The experimental time traces are slightly broadened by our temporal instrument response function due to the roughly thermal velocity distribution of our sampling expansion at the ionization region.[52] We empirically determine the width of this response function (∼0.5 ms at half-maximum) using the measured propene time trace at 530 K. The MSI model predicts with high confidence that at 530 K propene is formed exclusively via a very rapid formally direct propyl + O_2 reaction (see below) with a pseudo-first-order rate coefficient of $\sim 2 \times 10^4$ s^{-1}, and therefore its measured rise time at this temperature is due primarily to the instrumental response. To aid in comparison with experimental data, the time traces predicted by the MSI model in Figure 6 and afterward have been convolved with the experimental instrument response.

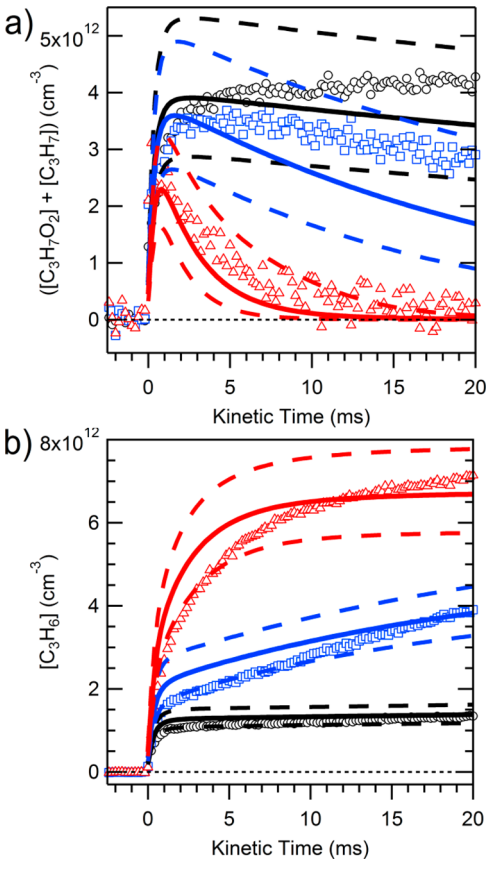

Figure 6. Concentration−time profiles of (a) m/z = 43 ions (mostly sum of n- and i-$C_3H_7O_2$) and (b) propene. The black, blue, and red colors represent T = 530, 600, and 670 K, respectively. Open symbols are experimental traces. Solid and dashed lines are modeling predictions and uncertainty bounds, respectively, convolved with our experimental time response function for comparison with experimental data. $C_3H_7O_2$ radicals were not experimentally quantified; their measured time profiles are scaled to the model results using temperature-dependent scaling constants.

Propene is the major closed-shell product observed at all temperatures and is formed mainly from HO_2 elimination via n-C_3H_7 + O_2 and i-C_3H_7 + O_2 reactions. The absolute photoionization cross-section of propyl peroxy radicals is not known, and therefore we do not quantify their concentration experimentally; instead, the $C_3H_7O_2$ signals in Figure 6 are scaled to match the model predictions. At 530 K, the time profiles of propyl peroxy radicals and propene exhibit a rapid rise followed by a plateau. At this temperature, a large fraction of the reactive flux from propyl + O_2 proceeds to stabilized propyl peroxy radicals, with the rest forming products, mostly propene + HO_2, by formally direct channels. Subsequent thermal decomposition of the stabilized $C_3H_7O_2$ radicals is slow on the experimental time scale, so that both $C_3H_7O_2$ and propene signals appear nearly constant. Predictions using the MSI model match the measured propene concentration well, but show marked differences from the experimental propyl peroxy signal. The model predicts a sharp rise of $C_3H_7O_2$, produced solely by the propyl + O_2 reaction within 1 ms after photolysis; this rise is followed by a gradual decay, mainly attributable at 530 K to the radical−radical reactions $C_3H_7O_2$ + HO_2 (∼50% of total consumption) and $C_3H_7O_2$ + $C_3H_7O_2$ (∼25%). The model predicts that unimolecular dissociation is responsible for only ∼10−20% of $C_3H_7O_2$ consumption at this temperature. Uncertainties in the rate coefficients for the n-/i-$C_3H_7O_2$ + HO_2 and n-/i-$C_3H_7O_2$ cross- and self-reactions may be responsible for the disparity between the measured long-time $C_3H_7O_2$ behavior and the model predictions. In addition, the differences at both early and late kinetic times may be due to experimental artifacts, e.g., potential contributions to the m/z = 43 ion signal from dissociative ionization of other compounds (possibly propyl hydroperoxides), which would interfere with the signal from $C_3H_7O_2$.

At 600 K prompt formation of propene is more prominent than at 530 K, because the nascent chemically activated $C_3H_7O_2$ radicals are formed with higher internal energies and because these higher-energy radicals are less efficiently stabilized by collisions. At later kinetic times, the $C_3H_7O_2$ time trace decays slowly, and the propene trace shows a secondary slow rise, mainly caused by thermal decomposition of $C_3H_7O_2$. Model predictions indicate that at 600 K the primary chemistry contributes over 70% to the total $C_3H_7O_2$ consumption, whereas the secondary n-/i-$C_3H_7O_2$ + HO_2 reactions contribute ∼20%. The model reproduces propene concentration well, and the differences between the model predictions and measured $C_3H_7O_2$ time profiles are likely caused by the same factors as above. At 670 K, thermal decomposition of propyl peroxy radicals becomes faster, and, under the time resolution of the present experiment, the separation in time scales for prompt and thermal product

DOI: 10.1021/acs.jpca.5b01008
J. Phys. Chem. A 2015, 119, 7116−7129

formation disappears. At this temperature, the model predicts that secondary reactions (RO_2 + RO_2 and RO_2 + HO_2) do not compete effectively with unimolecular decomposition of $C_3H_7O_2$ and contribute less than 7% to the total consumption. Although the predicted rise of propene and decay of $C_3H_7O_2$ are somewhat faster than the experimental measurements, overall, the model agrees fairly closely with the experiments. At time t = 20 ms, the experimentally determined yield of propene relative to $[Cl]_0$ is (20 ± 4)% at 530 K, (55 ± 11)% at 600 K, and (86 ± 17)% at 670 K. At the two lower temperatures, the propene yield reflects the presence of stabilized peroxy radicals, whereas at 670 K all $C_3H_7O_2$ has reacted away by 20 ms. Thus, our observed propene yield at 670 K is in good agreement with earlier observations by Baker et al.,[9] who found that ∼80% of propyl radicals are oxidized to propene at 753 K under their experimental conditions, and by Slagle et al.,[13] who found a final propene yield of >0.8 from the n-C_3H_7 + O_2 reaction at 635 K.

The prompt yield of propene via the formally direct pathway C_3H_7 + O_2 → C_3H_6 + HO_2 observed in the experiment is ∼15% at 530 K and ∼23% at 600 K, which compares well with MSI modeling predictions of 16% (530 K) and 25% (600 K). The remainder of the flux mainly goes to stabilized propyl peroxy radicals. The model also shows that backdissociation of n- and i-$C_3H_7O_2$ radicals to propyl + O_2 competes with decomposition to C_3H_6 + HO_2 at our experimental conditions. When formed by backdissociation of $C_3H_7O_2$, n- and i-C_3H_7 can react again with O_2 to yield either stabilized peroxy radicals or stable products, mostly C_3H_6 + HO_2. As a consequence, besides the initial formally direct channel

$$C_3H_7 + O_2 \rightarrow C_3H_6 + HO_2 \quad \text{(R9)}$$

propene formation from thermal decomposition of $C_3H_7O_2$ radicals occurs via two pathways:

$$C_3H_7O_2 \rightarrow C_3H_7 + O_2 \rightarrow C_3H_6 + HO_2 \quad \text{(R10)}$$

$$C_3H_7O_2 \rightarrow C_3H_6 + HO_2 \quad \text{(R11)}$$

where the second step in the indirect route R10 is formally direct HO_2 elimination (R9). Taking into account contributions from R9−R11 integrated up to 20 ms, the model predicts that the reactions of n- and i-C_3H_7 contribute nearly equally (50 ± 5)% to the total yield of C_3H_6 at all temperatures. The formally direct reaction R9 is entirely responsible for the prompt formation of propene, which is the only source of propene at low temperatures. Of the two thermal pathways, the forward route R11 is strongly favored at lower T, whereas R10 becomes increasingly dominant at high T.

C_3H_6O Isomers: Acetone, Propanal, Oxetane, Methyloxirane. Although the C_3H_6O isomers are formed in minor quantities relative to propene, they are key products in propyl oxidation, because their formation is linked with passage through key parts of the PES, such as the QOOH minima. The cyclic ethers methyloxirane and oxetane are produced only through isomerization to QOOH and thus serve as markers for these elusive intermediates. The carbonyl species acetone and propanal, on the other hand, can be formed either by secondary reactions of propyl peroxy radicals or by their thermal decomposition (see below); the primary unimolecular formation was not included in earlier models such as by Huang et al. due to high energetic barriers.[22] The experimental yields of all four C_3H_6O isomers at a kinetic time of 20 ms are shown in Table 2 and compared in Table 3 with results from the MSI model and the earlier model of Huang et al.[22]

Table 3. Experimental Concentrations at t = 20 ms of the C_3H_6O Isomers Acetone, Propanal, Oxetane, and Methyloxirane at 530, 600, and 670 K, Compared to Predictions from the Huang et al.,[22] *a priori*, and MSI Models

	concentration at t = 20 ms/10^{10} cm^{-3}			
	Huang et al.	*a priori*	MSI	exp
		T = 530 K		
acetone	4.3	3.6	$2.2\ ^{+6.8}/_{-1.7}$	1.4 ± 0.8
propanal	4.9	4.5	$2.3\ ^{+6.7}/_{-1.7}$	3.9 ± 0.9
oxetane	0	0.1	$0.29\ ^{+0.25}/_{-0.13}$	<0.17
methyloxirane	8.4	4.7	$4.3\ ^{+1.3}/_{-1.0}$	3.2 ± 0.9
		T = 600 K		
acetone	1.4	1.6	$1.1\ ^{+4.1}/_{-0.9}$	2.5 ± 0.9
propanal	2.3	2.6	$1.3\ ^{+4.4}/_{-1.0}$	8.3 ± 2.3
oxetane	0	0.6	$1.1\ ^{+0.7}/_{-0.4}$	1.0 ± 0.8
methyloxirane	42	19	$11.8\ ^{+3.5}/_{-2.7}$	9.8 ± 2.6
		T = 670 K		
acetone	0.16	0.4	$0.2\ ^{+0.7}/_{-0.2}$	1.1 ± 0.8
propanal	0.3	0.5	$0.2\ ^{+0.6}/_{-0.2}$	6.0 ± 1.6
oxetane	0	2.8	$3.2\ ^{+1.2}/_{-0.9}$	3.7 ± 1.5
methyloxirane	75	45	$22.4\ ^{+7.5}/_{-5.6}$	18.4 ± 4.2

Methyloxirane is the most abundant C_3H_6O isomer observed in the present experiments at 670 K, whereas at 530 and 600 K propanal is produced in comparable amount. The experimental yield of methyloxirane relative to $[Cl]_0$ shows a pronounced positive temperature dependence: (0.47 ± 0.13)% at 530 K, (1.4 ± 0.4)% at 600 K, and (2.2 ± 0.5)% at 670 K; however, its yield relative to propene at t = 20 ms is independent of temperature within the experimental uncertainty ((2.4 ± 1.1)% at 530 K, (2.5 ± 1.2)% at 600 K, and (2.6 ± 1.1)% at 670 K). This dependence is consistent with methyloxirane formation mainly by decomposition of propyl peroxy radicals and can be attributed to stabilization of $C_3H_7O_2$ at lower temperature. The MSI model predicts methyloxirane concentrations in good agreement with the experimental results (Table 3). A production analysis reveals a strong preference of methyloxirane formation from n-C_3H_7 compared to i-C_3H_7: at all three temperatures, over 90% of methyloxirane is produced from the n-C_3H_7 + O_2 reaction, and less than 10% from the i-C_3H_7 + O_2 reaction, in both cases via a combination of formally direct and thermal pathways.

As seen in Table 3, the Huang et al.[22] model overpredicts the measured methyloxirane yields. That model was optimized using measured OH formation from earlier low-pressure chlorine-initiated propane oxidation[19,22] and assuming that methyloxirane + OH was the dominant source of OH. The substantially lower yield of methyloxirane observed in our study implies that other significant channels to OH must exist. Baker et al.[9] report a yield of methyloxirane between 5% and 9% normalized to propane consumed at 753 K. Under our conditions, we find an experimental yield of methyloxirane of (2.2 ± 0.5)% at 670 K. Because our yield of methyloxirane relative to propene is temperature-independent between 530 and 670 K within the experimental uncertainty, it is reasonable to assume a similar ratio at 753 K. Furthermore, our propene yield of (86 ± 17)% at 670 K is similar to the propene yield of ∼80% observed by Baker et al. at 753 K. Based on these results,

DOI: 10.1021/acs.jpca.5b01008
J. Phys. Chem. A 2015, 119, 7116−7129

our methyloxirane yield is consistently lower than that of Baker et al., although the different pressures and initiation methods used (slowly reacting H_2/O_2 mixture by Baker et al.; pulsed-photolytic Cl production in our study) prevent a more rigorous comparison.

The sum concentration of the other three C_3H_6O isomers (acetone, propanal, and oxetane) is comparable to that of methyloxirane. This result is surprising, because, as shown in Figures 3 and 4, the saddle points leading to formation of acetone, propanal, and oxetane from propyl + O_2 are high in energy, and these product channels were considered unimportant in earlier theoretical kinetics studies.[7,22,28] Because these products from propyl + O_2 are linked with OH formation, the associated channels could at least in part compensate for the "missing" OH source in the model of Huang et al.

The only pathway to oxetane production from propyl + O_2 is n-C_3H_7 + O_2 → n-$C_3H_7O_2$ → QOOH-1 → oxetane + OH (see Figure 3). QOOH-1 ($CH_2CH_2CH_2OOH$) is the smallest possible γ-QOOH radical. Compared with other possible QOOH isomers, γ-QOOH radicals are better candidates for second O_2 addition: the barrier for RO_2 ⇄ γ-QOOH isomerization via an energetically favorable six-membered ring structure is low compared to decomposition of γ-QOOH (see Figure 3).[7,30] Therefore, second O_2 addition, eventually leading to radical chain branching, can effectively compete with thermal dissociation. Oxetane formation serves as a marker for QOOH-1 and therefore deserves special attention. Although at 530 K its experimental yield is negligibly small (upper limit of 0.02% of $[Cl]_0$ at 530 K at a reaction time of 20 ms), oxetane is present in measurable amounts at 600 and 670 K (Table 3). At 670 K its yield relative to $[Cl]_0$ is (0.45 ± 0.19)%, only a factor of 5 lower than the yield of methyloxirane. The yield of oxetane shows stronger positive temperature dependence than that of propene and methyloxirane, consistent with the saddle point that controls oxetane formation being higher in energy than those controlling methyloxirane and propene formation. The optimized energies of the key transition states relative to those of the n/i-C_3H_7 + O_2 reactants are E_{TS6} = 2.1 kcal mol^{-1} (QOOH-1 ↔ oxetane + OH); E_{TS3} = −0.4 kcal mol^{-1} (n-$C_3H_7O_2$ ↔ QOOH-2); E_{TS11} = 1.0 kcal mol^{-1} (i-$C_3H_7O_2$ ↔ QOOH-3); E_{TS4} = −4.1 kcal mol^{-1} (n-$C_3H_7O_2$ ↔ propene + HO_2); E_{TS12} = −5.1 kcal mol^{-1} (i-$C_3H_7O_2$ ↔ propene + HO_2). The corresponding *ab initio* calculated energies for those transition states were 2.9 kcal mol^{-1} (E_{TS6}); −0.2 kcal mol^{-1} (E_{TS3}); 1.2 kcal mol^{-1} (E_{TS11}); −2.7 kcal mol^{-1} (E_{TS4}); −4.2 kcal mol^{-1} (E_{TS12}).

Baker et al.[9] also reported the formation of oxetane. Their yield of 0.7% at 753 K is slightly higher than our determination of (0.45 ± 0.19)% at 670 K relative to $[Cl]_0$. As is the case for methyloxirane, a rigorous comparison of the yields in the two experiments is difficult because of the different initiation methods used. However, the higher yield observed by Baker et al. is consistent with the strong positive temperature dependence for oxetane formation observed in our experiments. Similarly, Cord et al.[23] detected oxetane in their recent jet-stirred reactor study on low-temperature propane oxidation. At 650 K, their measured yield of oxetane relative to methyloxirane of ∼20% is in good agreement with the ratio of (20 ± 13)% observed in our experiments at 670 K. The model of Cord et al. underpredicted the yield of oxetane significantly, which was rationalized by the dominance of the QOOH-1 + O_2 reaction under their conditions and the uncertainty in the barrier height for the QOOH-1 → oxetane + OH reaction.

The competition between O_2 addition and decomposition of γ-QOOH radicals is an important aspect of autoignition reactions, and the n-C_3H_7 + O_2 system is a prototype for this chemistry. In fact, experiments of Walker and co-workers[53] and Eskola et al.[54] show that analogous channels via γ-QOOH radicals to 2-methyloxetane + OH are prominent in the n-/sec-butyl + O_2 reactions. More recently, Eskola et al.[55] showed that ketohydroperoxide formation from n-butane oxidation resulted predominantly from O_2 addition to 4-hydroperoxy-2-butyl (the γ-QOOH radical in the 1-butyl + O_2 reaction). Although oxetane is a minor product in propane oxidation, our measurements quantify the yield of the associated channel in the propane oxidation model.

The measured concentrations of acetone and propanal show nonmonotonic temperature dependence and are highest at 600 K. The exact sources of these carbonyl species are difficult to pinpoint, though it appears that known primary pathways in propyl + O_2 (TS13: i-propyl + O_2 → OH + acetone and TS5: n-propyl + O_2 → OH + propanal) are unable to completely explain their production. For example, trial optimizations that included acetone and propanal at 670 K as targets of the MSI model resulted in a 3.0 kcal mol^{-1} lower barrier height for TS13 and a 3.8 kcal mol^{-1} lower barrier height for TS5. This adjustment, required to reproduce the experimental measurements even at the highest temperatures, where these channels are most prominent, is beyond the estimated uncertainties in TS5. Furthermore, acetone and propanal formation through TS13 and TS5, both of which lie above the propyl + O_2 reactants in energy, would be expected to result in a monotonic temperature dependence of their yields.

An alternative explanation for the observed acetone and propanal yields might be missing pathways for their formation from propyl + O_2. For example, concerted 1,2-H atom transfer and OH loss from QOOH-2 (or QOOH-3) would lead to propanal (or acetone) + OH. Such saddle points were reported by Huynh et al.,[28] but the energies obtained at the CBS-QB3 level of theory are prohibitively high. Preliminary calculations on analogous saddle points in n-butane oxidation leading to butanal + OH show that these saddle points have an electronic structure that is very challenging to describe.[56] Limited further explorations using density functional theory[34] did not find any low-lying saddle points: barriers for identified saddle points for QOOH-1 → OH + propanal, QOOH-2 → OH + propanal, and QOOH-3 → OH + acetone were calculated to be 22.2, 21.1, and 23.7 kcal mol^{-1}, respectively.

One further possible source for acetone and propanal production is secondary chemistry, perhaps involving self- and cross-reactions of n-/i-$C_3H_7O_2$ and cross-reactions of n-/i-$C_3H_7O_2$ and n-/i-C_3H_7. In fact, our model suggests that acetone and propanal are produced largely from n-/i-$C_3H_7O_2$ + n-/i-$C_3H_7O_2$ reactions (as shown in Figure 7), particularly at lower temperatures, and the experimental observation of propanol isomers corroborates this assignment. However, knowledge of the kinetics of the $C_3H_7O_2$ + $C_3H_7O_2$ and C_3H_7 + $C_3H_7O_2$ reactions is rather limited. For example, while there are some measurements for total rate coefficients for n-$C_3H_7O_2$ + n-$C_3H_7O_2$ and i-$C_3H_7O_2$ + i-$C_3H_7O_2$ reactions near 300 K,[47] their temperature and pressure dependence or product branching ratios are considerably less characterized. A definitive conclusion regarding the sources of acetone and propanal

DOI: 10.1021/acs.jpca.5b01008
J. Phys. Chem. A 2015, 119, 7116−7129

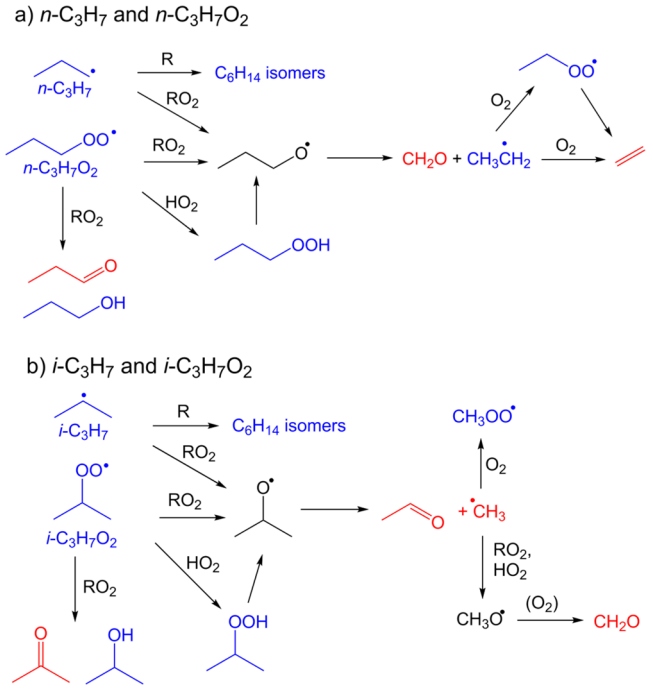

Figure 7. Reaction scheme for main secondary radical−radical reactions originating from (a) n-C_3H_7 or n-$C_3H_7O_2$ and (b) i-C_3H_7 or i-$C_3H_7O_2$. R is either n- or i-C_3H_7, and RO_2 is either n- or i-$C_3H_7O_2$. The color code indicates that a species was either not detected (black), detected but not quantified (blue), or detected and quantified (red).

under our conditions requires further investigations of the possible primary and secondary pathways to their formation.

Secondary Products. Products other than propene, C_3H_7, $C_3H_7O_2$, and the C_3H_6O isomers are formed via secondary chemistry, except CH_3 and C_2H_4, which are formed to some extent via thermal decomposition of n-C_3H_7 at higher temperatures. The experimental time profiles and MSI model predictions for the main secondary products are shown in Figure 8. In general, the model describes the radical−radical chemistry well and provides valuable insight into the formation and consumption pathways of the important secondary species, as summarized in Figure 7. The reactions that are responsible for the production of all of the experimentally measured secondary products are listed in Table S11 along with their rate coefficients, evaluated at our experimental conditions.

Most of the secondary reactions in the initial stages of propane oxidation involve propyl, propyl peroxy, and HO_2 radicals, and generate propyl hydroperoxides and propoxy radical intermediates. Propyl hydroperoxide (C_3H_7OOH) is formed mostly from $C_3H_7O_2 + HO_2$ reactions. Experimentally, we do not separate the n- and i-C_3H_7OOH isomers or quantify their yields, because their photoionization calibration spectra are unknown. Whereas at 530 and 600 K C_3H_7OOH is stable on the experimental time scale, its time profile becomes transient at 670 K, reflecting thermal dissociation. The dominant decomposition reaction is fission of the O−O bond, adding to the formation of OH and propoxy radicals: n-$C_3H_7OOH \rightarrow n$-C_3H_7O (n-propoxy) + OH and i-$C_3H_7OOH \rightarrow i$-C_3H_7O (i-propoxy) + OH. The minor presence of propanol isomers (C_3H_7OH) reflects the disproportionation channel in self- and cross-reactions of propyl peroxy radicals ($RO_2 + RO_2 \rightarrow R_{-H}O + ROH + O_2$). In addition, we observe minor formation of H_2O_2, for which the model identifies the self-reaction of HO_2 ($2\ HO_2 \rightarrow H_2O_2 + O_2$) as the dominant source. Note that the largest photon energy employed in our study (11.2 eV) is not sufficient to ionize HO_2 (IE(HO_2) = 11.35 eV).[57]

Both n- and i-propoxy radicals are intermediates for the formation of most of the other secondary products observed. In addition to thermal decomposition of propyl hydroperoxide, C_3H_7O is formed by the reactions $C_3H_7 + C_3H_7O_2$ at early kinetic times, when the concentration of propyl radicals is sufficiently high. On a longer time scale, propoxy radicals are formed by self- and cross-reactions of $C_3H_7O_2$ and by the reaction $C_3H_7O_2 + CH_3 \rightarrow C_3H_7O + CH_3O$. Thermal decomposition of propoxy radicals via β-CC bond fission reactions at 4 Torr and $T > 500$ K is very rapid, with rate coefficients in excess of 10^5 s^{-1}.[58] The rate coefficients for the competing n-/i-propoxy + O_2 reaction are on the order of 10^{-14} cm^3 s^{-1} at these conditions.[59] With O_2 concentrations of 1×10^{16} cm^{-3}, unimolecular decomposition of n-/i-propoxy in our experiments is 3 orders of magnitude faster than their reaction with oxygen. As a consequence, reaction of the propoxy radicals proceeds almost exclusively via β-CC bond scission reactions: n-$C_3H_7O \rightarrow CH_2O + C_2H_5$ and i-$C_3H_7O \rightarrow CH_3CHO + CH_3$.[58] Because of their fast decomposition, we do not observe the propoxy radicals (measured IE of 9.20 eV[60]) themselves, although we detect their β-scission products: ethyl, formaldehyde, acetaldehyde, and methyl.

Ethyl radicals are formed exclusively by decomposition of n-propoxy and removed mainly by reaction with O_2. This reaction is the main source of ethene, either via the formally direct pathway $C_2H_5 + O_2 \rightarrow C_2H_4 + HO_2$ or via thermal decomposition of stabilized ethyl peroxy radicals, at 530 and 600 K. At 670 K, formation of C_2H_4 from unimolecular decomposition of n-C_3H_7 radicals via β-CC bond fission (n-$C_3H_7 \rightarrow C_2H_4 + CH_3$) is as important as formation via $C_2H_5 + O_2$. Predictions of the MSI model are generally in good agreement with the experimental time traces, although at 670 K we observe more C_2H_4 than the model predicts.

The MSI model reproduces the time profile of CH_2O well at 530 K, although it predicts less CH_2O than observed at higher temperatures. Beside decomposition of n-C_3H_7O, other important pathways to CH_2O are reactions of methoxy (CH_3O) radicals: $CH_3O + O_2 \rightarrow CH_2O + HO_2$ and $CH_3O \rightarrow CH_2O + H$. Methoxy radicals themselves are formed mostly via reactions of CH_3 with propyl peroxy at 530 K, and mostly by $CH_3 + HO_2 \rightarrow CH_3O + OH$ at 670 K.

According to the MSI model, acetaldehyde is formed exclusively from decomposition of i-C_3H_7O. The model predictions and experimental measurements are generally in very good agreement for all temperatures. CH_3 radicals are formed from decomposition of i-C_3H_7O (and also from decomposition of n-C_3H_7 at higher temperature) and are consumed by reaction with a variety of species. At lower temperature $C_3H_7O_2 + CH_3 \rightarrow C_3H_7O + CH_3O$ is the dominant consumption reaction, with contributions from the reaction $CH_3 + O_2 \rightarrow CH_3O_2$. The $CH_3 + HO_2 \rightarrow CH_3O + OH$ reaction, relatively unimportant at 530 K, becomes the major sink of CH_3 radicals at 670 K and furthermore an important source of OH on a longer time scale. MSI model predictions overestimate the experimental CH_3 yield at lower temperatures but are reasonably consistent with measurements at higher temperatures.

DOI: 10.1021/acs.jpca.5b01008
J. Phys. Chem. A 2015, 119, 7116−7129

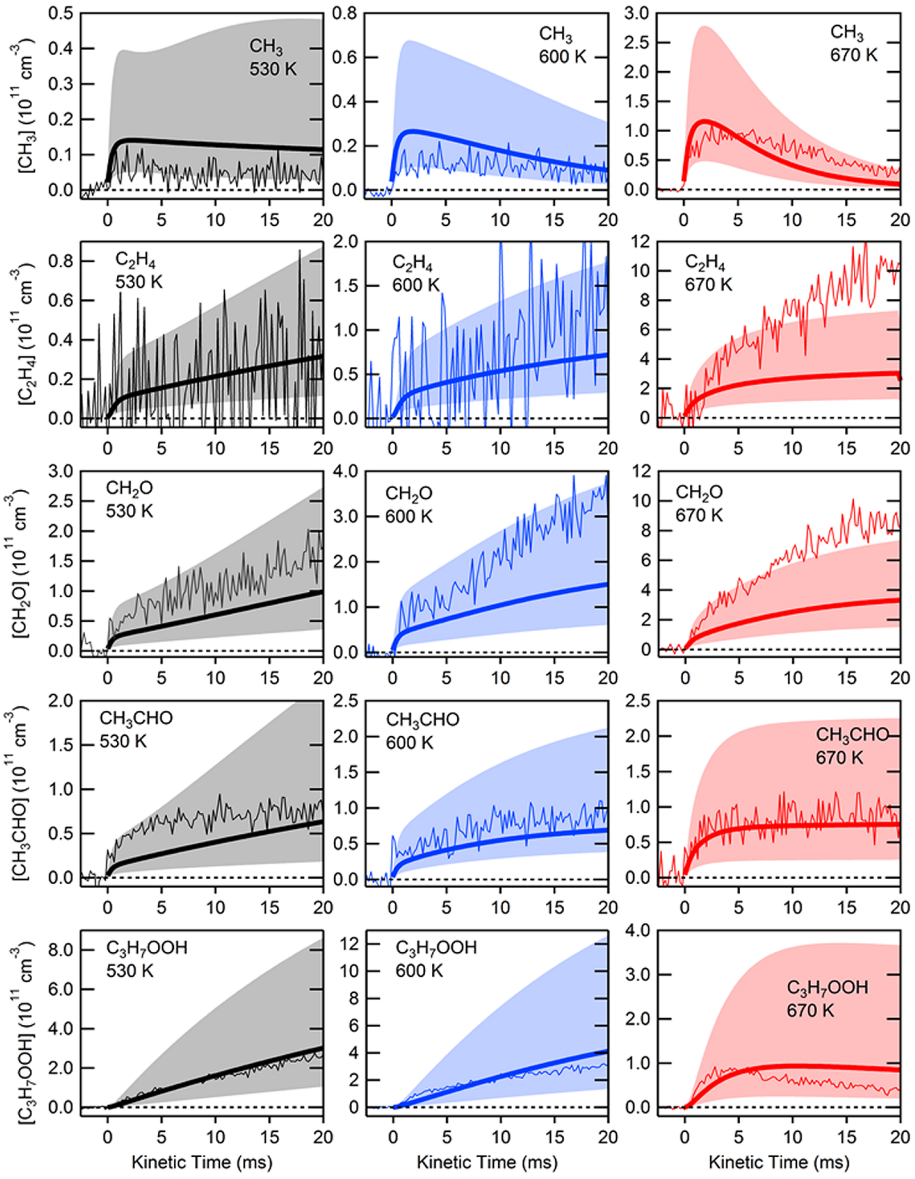

Figure 8. Secondary products of propane oxidation: CH_3, C_2H_4, CH_2O, CH_3CHO, and C_3H_7OOH. Experimental time profiles (thin lines) are plotted along with MSI model predictions (thick lines) in black (530 K), blue (600 K), and red (670 K). The model uncertainty bounds are shown by the shaded areas in each plot. The model predictions and uncertainties are convolved with our experimental time response function. Because C_3H_7OOH was not quantified experimentally, its experimental traces are scaled for comparison with model predictions.

■ CONCLUSIONS AND OUTLOOK

We have observed in real-time the formation of intermediates and products from Cl-initiated propane oxidation at 4 Torr and at temperatures of 530, 600, and 670 K using isomer-resolved MPIMS. The experimental time traces of the products formed in the *n*-C_3H_7 + O_2 and *i*-C_3H_7 + O_2 reactions reveal a temperature-dependent competition between rapid (formally direct) product formation and thermal decomposition of stabilized propyl peroxy radicals. Formation of propene via HO_2 elimination from both *n*- and *i*-propyl peroxy radicals is the dominant product channel under our conditions. The experimental measurements for methyloxirane and oxetane are consistent with their formation from primary C_3H_7 + O_2 chemistry in conjunction with the OH radical. The multiscale informatics approach, used to model and interpret the experimental results, reproduces the yields of most species quantified and captures the competition between prompt and thermal product formation. To rationalize the experimental yields of propanal and acetone, the saddle-point energies for the reactions *n*-$C_3H_7O_2$ → propanal + OH and *i*-$C_3H_7O_2$ → acetone + OH would have to be lowered by unreasonably large amounts (3.0 and 3.8 kcal mol^{-1}, respectively), compared to previously published results from high-level quantum-chemical calculations.[7] Such adjustments are well outside the estimated uncertainty of these calculations, which suggests that other unexplored pathways to carbonyl formation in low-temperature alkane oxidation might exist.

The results from this study form the basis for an investigation of low-temperature propane oxidation at higher pressure, which will help further constrain and refine the kinetic model used to interpret our results. Such studies, using a new high-pressure reactor coupled to synchrotron-based MPIMS detection, are currently underway.

DOI: 10.1021/acs.jpca.5b01008
J. Phys. Chem. A 2015, 119, 7116−7129

■ ASSOCIATED CONTENT

Supporting Information

Figure S1: Comparison of the m/z = 42 photoionization product spectrum with a propene calibration spectrum. Figure S2: Time behavior of the m/z = 43 ($C_3H_7^+$) ion signal at 530 K and 4 Torr as a function of photoionization energy. Tables S1−S4: Photoionization cross sections of propane, acetone, methyloxirane and oxetane; Tables S5−S7: Experimental concentration−time profiles of all species quantified. Tables S8−S10: Experimental intensity-time profiles for all species identified but not quantified. Table S11: Sub-mechanism of secondary product formation. This material is available free of charge via the Internet at http://pubs.acs.org.

■ AUTHOR INFORMATION

Corresponding Authors

*Oliver Welz: e-mail: oliver.welz@uni-due.de; phone: +49(203)379-1888.

*Leonid Sheps: e-mail: lsheps@sandia.gov; phone: +1(925) 294-2927.

Present Addresses

[‖]Institute for Combustion and Gas Dynamics, University of Duisburg-Essen, Duisburg, Germany.

[⊥]School of Engineering, Brown University, Providence, RI 02912, USA.

Notes

The authors declare no competing financial interest.

■ ACKNOWLEDGMENTS

We thank Mr. Howard Johnsen (Sandia) and the staff at the Chemical Dynamics Beamline at the ALS for excellent technical support of these experiments. This work was supported by the U.S. Department of Energy, Office of Basic Energy Sciences, Division of Chemical Sciences, Geosciences, and Biosciences. The work at Argonne National Laboratory was supported under contract DE-AC02-06CH11357. Sandia is a multiprogram laboratory operated by Sandia Corporation, a Lockheed Martin Company, for the National Nuclear Security Administration, under contract DE-AC04-94AL85000. The work of O.W., M.P.B., C.F.G., S.J.K., C.A.T., and L.S. was part of the Argonne-Sandia Consortium on High-Pressure Combustion Chemistry. M.P.B. and C.F.G. were also supported by Director's Postdoctoral Fellowships from Argonne National Lab. The Advanced Light Source is supported by the Director, Office of Science, BES/DOE, under contract DE-AC02-05CH11231 between Lawrence Berkeley National Laboratory and the DOE.

■ REFERENCES

(1) Zádor, J.; Taatjes, C. A.; Fernandes, R. X. Kinetics of Elementary Reactions in Low-Temperature Autoignition Chemistry. *Prog. Energy Combust. Sci.* **2011**, *37*, 371−421.

(2) Westbrook, C. K. Chemical Kinetics of Hydrocarbon Ignition in Practical Combustion Systems. *Proc. Combust. Inst.* **2000**, *28*, 1563−1577.

(3) Dec, J. E. Advanced Compression-Ignition Engines - Understanding the In-Cylinder Processes. *Proc. Combust. Inst.* **2009**, *32*, 2727−2742.

(4) Rienstra-Kiracofe, J. C.; Allen, W. D.; Schaefer, H. F., III. The C_2H_5 + O_2 Reaction Mechanism: High-Level Ab Initio Characterizations. *J. Phys. Chem. A* **2000**, *104*, 9823−9840.

(5) Ignatyev, I. S.; Xie, Y.; Allen, W. D.; Schaefer, H. F., III. Mechanism of the C_2H_5 + O_2 Reaction. *J. Chem. Phys.* **1997**, *107*, 141−155.

(6) Zádor, J.; Huang, H.; Welz, O.; Zetterberg, J.; Osborn, D. L.; Taatjes, C. A. Directly Measuring Reaction Kinetics of QOOH − A Crucial but Elusive Intermediate in Hydrocarbon Autoignition. *Phys. Chem. Chem. Phys.* **2013**, *15*, 10753−10760.

(7) Goldsmith, C. F.; Green, W. H.; Klippenstein, S. J. Role of O_2 + QOOH in Low-Temperature Ignition of Propane. 1. Temperature and Pressure Dependent Rate Coefficients. *J. Phys. Chem. A* **2012**, *116*, 3325−3346.

(8) Goldsmith, C. F.; Burke, M. P.; Georgievskii, Y.; Klippenstein, S. J. Effect of Non-Thermal Product Energy Distributions on Ketohydroperoxide Decomposition Kinetics. *Proc. Comb. Inst.* **2015**, *35*, 283−290.

(9) Baker, R. R.; Baldwin, R. R.; Walker, R. W. Addition of C_3H_8 to Slowly Reacting Mixtures of Hydrogen and Oxygen at 480°C. Reactions of Propyl Radical. *Trans. Faraday Soc.* **1970**, *66*, 3016−3031.

(10) Baldwin, R. R.; Walker, R. W.; Yorke, D. A. Reaction of n-Propyl Radicals with Oxygen, Hydrogen and Deuterium. *J. Chem. Soc., Faraday Trans. I* **1973**, *69*, 826−832.

(11) Baldwin, R. R.; Cleugh, C. J.; Walker, R. W. Reactions of iso-Propyl Radicals with Oxygen, Hydrogen and Deuterium. *J. Chem. Soc., Faraday Trans. 1* **1976**, *72*, 1715−1722.

(12) Ruiz, R. P.; Bayes, K. D. Rates of Reaction of Propyl Radicals with Molecular Oxygen. *J. Phys. Chem.* **1984**, *88*, 2592−2595.

(13) Slagle, I. R.; Park, J.-Y.; Gutman, D. Experimental Investigation of the Kinetics and Mechanism of the Reaction of n-Propyl Radicals with Molecular Oxygen from 297 to 635 K. *Symp. (Int.) Combust., [Proc.]* **1985**, *20*, 733−741.

(14) Slagle, I. R.; Ratajczak, E.; Heaven, M. C.; Gutman, D.; Wagner, A. F. Kinetics of Polyatomic Free-Radicals Produced by Laser Photolysis. 5. Study of the Equilibrium *i*-C_3H_7 + O_2 ↔ *i*-$C_3H_7O_2$ between 592 and 692 K. *J. Am. Chem. Soc.* **1985**, *107*, 1838−1845.

(15) Gulati, S. K.; Walker, R. W. Arrhenius parameters for the reaction *i*-C_3H_7 + O_2 = C_3H_6 + HO_2. *J. Chem. Soc. Faraday Trans. 2* **1988**, *84*, 401−407.

(16) Kaiser, E. W.; Wallington, T. J. Formation of C_3H_6 from the Reaction C_3H_7 + O_2 and C_2H_3Cl from C_2H_4Cl + O_2 at 297 K. *J. Phys. Chem.* **1996**, *100*, 18770−18774.

(17) Kaiser, E. W. Formation of C_3H_6 from the Reaction C_3H_7 + O_2 between 450 and 550 K. *J. Phys. Chem. A* **1998**, *102*, 5903−5906.

(18) DeSain, J. D.; Clifford, E. P.; Taatjes, C. A. Infrared Frequency-Modulation Probing of Product Formation in Alkyl + O_2 Reactions: II. The Reaction of C_3H_7 with O_2 between 295 and 683 K. *J. Phys. Chem. A* **2001**, *105*, 3205−3213.

(19) DeSain, J. D.; Klippenstein, S. J.; Miller, J. A.; Taatjes, C. A. Measurements, Theory, and Modeling of OH Formation in Ethyl + O_2 and Propyl + O_2 Reactions. *J. Phys. Chem. A* **2003**, *107*, 4415−4427.

(20) Estupiñán, E. G.; Klippenstein, S. J.; Taatjes, C. A. Measurements and Modeling of HO_2 Formation in the Reactions of n-C_3H_7 and i-C_3H_7 Radicals with O_2. *J. Phys. Chem. B* **2005**, *109*, 8374−8387.

(21) Estupiñán, E. G.; Smith, J. D.; Tezaki, A.; Jusinski, L. E.; Klippenstein, S. J.; Taatjes, C. A. Measurements and Modeling of DO_2 Formation in the Reactions of C_2D_5 and C_3D_7 Radicals with O_2. *J. Phys. Chem. A* **2007**, *111*, 4015−4030.

(22) Huang, H.; Merthe, D. J.; Zádor, J.; Jusinski, L. E.; Taatjes, C. A. New Experiments and Validated Master-Equation Modeling for OH Production in Propyl + O_2 Reactions. *Proc. Comb. Inst.* **2011**, *33*, 293−299.

(23) Cord, M.; Husson, B.; Lizardo Huerta, J. C.; Herbinet, O.; Glaude, P. A.; Fournet, R.; Sirjean, B.; Battin-Leclerc, F.; Ruiz-Lopez, M.; Wang, Z.; et al. Study of the Low Temperature Oxidation of Propane. *J. Phys. Chem. A* **2012**, *116*, 12214−28.

(24) DeSain, J. D.; Taatjes, C. A.; Miller, J. A.; Klippenstein, S. J.; Hahn, D. K. Infrared Frequency-Modulation Probing of Product Formation in Alkyl + O_2 Reactions: IV. Reactions of Propyl and Butyl Radicals with O_2. *Faraday Discuss.* **2001**, *119*, 101−120.

DOI: 10.1021/acs.jpca.5b01008
J. Phys. Chem. A 2015, 119, 7116−7129

(25) Wijaya, C. D.; Sumathi, R.; Green, W. H., Jr. Thermodynamic Properties and Kinetic Parameters for Cyclic Ether Formation from Hydroperoxyalkyl Radicals. *J. Phys. Chem. A* **2003**, *107*, 4908−4920.
(26) Green, W. H.; Wijaya, C. D.; Yelvington, P. E.; Sumathi, R. Predicting Chemical Kinetics with Computational Chemistry: is QOOH → HOQO Important in Fuel Ignition? *Mol. Phys.* **2004**, *102*, 371−380.
(27) Merle, J. K.; Hayes, C. J.; Zalyubovsky, S. J.; Glover, B. G.; Miller, T. A.; Hadad, C. M. Theoretical Determinations of the Ambient Conformational Distribution and Unimolecular Decomposition of n-Propylperoxy Radical. *J. Phys. Chem. A* **2005**, *109*, 3637−3646.
(28) Huynh, L. K.; Carstensen, H.-H.; Dean, A. M. Detailed Modeling of Low-Temperature Propane Oxidation: 1. The Role of the Propyl + O_2 Reaction. *J. Phys. Chem. A* **2010**, *114*, 6594−6607.
(29) Zhang, F.; Dibble, T. S. Impact of Tunneling on Hydrogen-Migration of the n-Propylperoxy Radical. *Phys. Chem. Chem. Phys.* **2011**, *13*, 17969−17977.
(30) Miyoshi, A. Systematic Computational Study on the Unimolecular Reactions of Alkylperoxy (RO_2), Hydroperoxyalkyl (QOOH), and Hydroperoxyalkylperoxy (O_2QOOH) Radicals. *J. Phys. Chem. A* **2011**, *115*, 3301−3325.
(31) Burke, M. P.; Goldsmith, C. F.; Georgievskii, Y.; Klippenstein, S. J. Towards a Quantitative Understanding of the Role of Non-Boltzmann Reactant Distributions in Low Temperature Oxidation. *Proc. Comb. Inst.* **2015**, *35*, 205−213.
(32) DeSain, J. D.; Klippenstein, S. J.; Miller, J. A.; Taatjes, C. A. Corrigendum: Measurements, Theory, and Modeling of OH Formation in Ethyl + O_2 and Propyl + O_2 Reactions. *J. Phys. Chem. A* **2004**, *108*, 7127−7128.
(33) Burke, M. P.; Klippenstein, S. J.; Harding, L. B. A Quantitative Explanation for the Apparent Anomalous Temperature Dependence of OH + HO_2 = H_2O + O_2 Through Multi-Scale Modeling. *Proc. Comb. Inst.* **2013**, *34*, 547−555.
(34) Burke, M. P.; Goldsmith, C. F.; Klippenstein, S. J.; Welz, O.; Huang, H.; Antonov, I. O.; Savee, J. D.; Osborn, D. L.; Zádor, J.; Taatjes, C. A.; Sheps, L. Multiscale Informatics for Low-Temperature Propane Oxidation: Further Complexities in Studies of Complex Reactions. *J. Phys. Chem. A* **2015**, DOI: 10.1021/acs.jpca.5b01003.
(35) Osborn, D. L.; Zou, P.; Johnsen, H.; Hayden, C. C.; Taatjes, C. A.; Knyazev, V. D.; North, S. W.; Peterka, D. S.; Ahmed, M.; Leone, S. R. The Multiplexed Chemical Kinetic Photoionization Mass Spectrometer: A New Approach for Isomer Resolved Chemical Kinetics. *Rev. Sci. Instrum.* **2008**, *79*, 104103.
(36) Taatjes, C. A.; Hansen, N.; Osborn, D. L.; Kohse-Höinghaus, K.; Cool, T. A.; Westmoreland, P. R. "Imaging" Combustion Chemistry *via* Multiplexed Synchrotron-Photoionization Mass Spectrometry. *Phys. Chem. Chem. Phys.* **2008**, *10*, 20−34.
(37) Savee, J. D.; Soorkia, S.; Welz, O.; Selby, T. M.; Taatjes, C. A.; Osborn, D. L. Absolute Photoionization Cross-Section of the Propargyl Radical. *J. Chem. Phys.* **2012**, *136*, 134307.
(38) Ghosh, B.; Papanastasiou, D. K.; Burkholder, J. B. Oxalyl Chloride, ClC(O)C(O)Cl: UV/Vis Spectrum and Cl Atom Photolysis Quantum Yields at 193, 248, and 351 nm. *J. Chem. Phys.* **2012**, *137*, 164315.
(39) Welz, O.; Zádor, J.; Savee, J. D.; Sheps, L.; Osborn, D. L.; Taatjes, C. A. Low-Temperature Combustion Chemistry of n-Butanol: Principal Oxidation Pathways of Hydroxybutyl Radicals. *J. Phys. Chem. A* **2013**, *117*, 11983−12001.
(40) Welz, O.; Zádor, J.; Savee, J. D.; Ng, Y.-H.; Meloni, G.; Fernandes, R. X.; Sheps, L.; Simmons, B. A.; Lee, T. S.; Osborn, D. L.; et al. Low-Temperature Combustion Chemistry of Biofuels: Pathways in the Initial Low-Temperature (550 K − 750 K) Oxidation Chemistry of Isopentanol. *Phys. Chem. Chem. Phys.* **2012**, *14*, 3112−3127.
(41) Cooper, G.; Anderson, J. E.; Brion, C. E. Absolute Photoabsorption and Photoionization of Formaldehyde in the VUV and Soft X-Ray Regions (3−200 eV). *Chem. Phys.* **1996**, *209*, 61−77.
(42) Dodson, L. G.; Shen, L.; Savee, J. D.; Eddingsaas, N. C.; Welz, O.; Taatjes, C. A.; Osborn, D. L.; Sander, S. P.; Okumura, M. VUV Photoionization Cross Sections of HO_2, H_2O_2, and H_2CO. *J. Phys. Chem. A* **2015**, *119*, 1279−91.
(43) Welz, O.; Savee, J. D.; Eskola, A. J.; Sheps, L.; Osborn, D. L.; Taatjes, C. A. Low-Temperature Combustion Chemistry of Biofuels: Pathways in the Low-Temperature (550−700K) Oxidation Chemistry of Isobutanol and *tert*-Butanol. *Proc. Comb. Inst.* **2013**, *34*, 493−500.
(44) Lias, S. G. Ionization Energy Evaluation. In *NIST Chemistry WebBook*, NIST Standard Reference Database Number 69; Linstrom, P. J.; Mallard, W. G., Eds.; National Institute of Standards and Technology: Gaithersburg, MD, 2009.
(45) Choi, N.; Pilling, M.; Seakins, P.; Wang, L. Studies of Site Selective Hydrogen Atom Abstractions by Cl Atoms From Isobutane and Propane by Laser Flash Photolysis/IR Diode Laser Spectroscopy. *Phys. Chem. Chem. Phys.* **2006**, *8*, 2172−2178.
(46) Tyndall, G.; Orlando, J.; Wallington, T.; Dill, M.; Kaiser, E. Kinetics and Mechanisms of the Reactions of Chlorine Atoms with Ethane, Propane, and n-Butane. *Int. J. Chem. Kinet.* **1997**, *29*, 43−55.
(47) Atkinson, R.; Baulch, D.; Cox, R.; Crowley, J.; Hampson, R.; Hynes, R.; Jenkin, M.; Rossi, M.; Troe, J.; Subcommittee, I. Evaluated Kinetic and Photochemical Data for Atmospheric Cchemistry: Volume II - Gas Phase Reactions of Organic Species. *Atmos. Chem. Phys.* **2006**, *6*, 3625−4055.
(48) Sarzynski, D.; Sztuba, B. Gas-Phase Reactions of Cl Atoms with Propane, n-Butane, and Isobutane. *Int. J. Chem. Kinet.* **2002**, *34*, 651−658.
(49) Meloni, G.; Selby, T. M.; Goulay, F.; Leone, S. R.; Osborn, D. L.; Taatjes, C. A. Photoionization of 1-Alkenylperoxy and Alkylperoxy Radicals and a General Rule for the Stability of Their Cations. *J. Am. Chem. Soc.* **2007**, *129*, 14019−14025.
(50) Meloni, G.; Zou, P.; Klippenstein, S. J.; Ahmed, M.; Leone, S. R.; Taatjes, C. A.; Osborn, D. L. Energy-Resolved Photoionization of Alkyl Peroxy Radicals and the Stability of Their Cations. *J. Am. Chem. Soc.* **2006**, *128*, 13559−13567.
(51) Dyke, J.; Ellis, A.; Jonathan, N.; Morris, A. Vacuum Ultraviolet Photoelectron Spectroscopy of Transient Species. Part 18.-The Cyclopropyl, i-propyl and n-Propyl Radicals. *J. Chem. Soc., Faraday Trans. 2* **1985**, *81*, 1573−1586.
(52) Taatjes, C. A. How Does the Molecular Velocity Distribution Affect Kinetics Measurements by Time-Resolved Mass Spectrometry? *Int. J. Chem. Kinet.* **2007**, *39*, 565−570.
(53) Baker, R. R.; Baldwin, R. R.; Fuller, A. R.; Walker, R. W. Addition of n-C_4H_{10} and C_4H_8 to Slowly Reacting Mixtures of Hydrogen and Oxygen at 480°C. Part 1. Formation of Hydrocarbon Products. *J. Chem. Soc., Faraday Trans. 1* **1975**, *71*, 736−755.
(54) Eskola, A. J.; Welz, O.; Savee, J. D.; Osborn, D. L.; Taatjes, C. A. Synchrotron Photoionization Mass Spectrometry Measurements of Product Formation in Low-Temperature n-Butane Oxidation: Toward a Fundamental Understanding of Autoignition Chemistry and n-C_4H_9 + O_2/s-C_4H_9 + O_2 Reactions. *J. Phys. Chem. A* **2013**, *117*, 12216−35.
(55) Eskola, A. J.; Welz, O.; Zádor, J.; Antonov, I. O.; Sheps, L.; Savee, J. D.; Osborn, D. L.; Taatjes, C. A. Probing the Low-Temperature Chain-Branching Mechanism of *n*-Butane Autoignition Chemistry via Time-Resolved Measurements of Ketohydroperoxide Formation in Photolytically Initiated *n*-C_4H_{10} Oxidation. *Proc. Comb. Inst.* **2015**, *35*, 291−298.
(56) Welz, O.; Klippenstein, S. J.; Harding, L. B.; Taatjes, C. A.; Zádor, J. Unconventional Peroxy Chemistry in Alcohol Oxidation: The Water Elimination Pathway. *J. Phys. Chem. Lett.* **2013**, *4*, 350−354.
(57) Litorja, M.; Ruscic, B. A Photoionization Study of the Hydroperoxyl Radical, HO_2, and Hydrogen Peroxide, H_2O_2. *J. Electron Spectrosc. Relat. Phenom.* **1998**, *97*, 131−146.
(58) Zador, J.; Miller, J. A. Unimolecular Dissociation of Hydroxypropyl and Propoxy Radicals. *Proc. Comb. Inst.* **2013**, *34*, 519−526.
(59) Atkinson, R. Atmospheric Reactions of Alkoxy and Beta-hydroxyalkoxy Radicals. *Int. J. Chem. Kinet.* **1997**, *29*, 99−111.
(60) Williams, J. M.; Hamill, W. H. Ionization Potentials of Molecules and Free Radicals and Appearance Potentials by Electron Impact in Mass Spectrometer. *J. Chem. Phys.* **1968**, *49*, 4467−4477.

DOI: 10.1021/acs.jpca.5b01008
J. Phys. Chem. A 2015, 119, 7116−7129

NOTE ADDED AFTER ASAP PUBLICATION

There were errors in the reference mentioned in the Abstract and ref 34 in the version published ASAP May 1, 2015; the corrected version was published ASAP June 8, 2015.

DOI: 10.1021/acs.jpca.5b01008
J. Phys. Chem. A 2015, 119, 7116−7129